

# NUMERICAL INVESTIGATION OF GDL COMPRESSION RATE ON AIR-BREATHING PROTON EXCHANGE MEMBRANE FUEL CELL

Tingting Sun, Biao Xie, Fan Zhang, Lizhen Wu, Kui Jiao\*

State Key Laboratory of Engines, Tianjin University, 135 Yaguan Rd, Tianjin, China, 300350

\*Corresponding author: kjiao@tju.edu.cn; tel: +86-22-27404460; fax: +86-22-27383362

## ABSTRACT

In this study, a 3D (three-dimensional) multiphase CFD (computational fluid dynamics) model of AB-PEMFC (air-breathing proton exchange membrane fuel cell) is developed, in which the influence of GDL compression is considered. The anisotropic electric and thermal conductivities in the in-plane and through-plane directions of GDLs and the contact resistance between GDL and BP (bipolar plate) are also included in this model. It was found that the optimal open area ratio for the maximum performance of AB-PEMFC is different under different GDL compression rates, and generally the larger the compression rate is, the larger the optimal open area ratio.

**Keywords:** AB-PEMFC, GDL compression rate, 3D multiphase model, Open area ratio

## 1. INTRODUCTION

Compared with the traditional PEMFC, the cathode of AB-PEMFC is directly open to the air to obtain oxygen through natural convection, which features simple system and gets rid of the sub-systems of gas supply, humidification and cooling. Thanks to the small volume and weight, it is usually used as a portable power source [2].

So far numerous researches have been carried out on the AB-PEMFC. For example, Jeong et al. [3] studied the influence of the relative humidity (RH) of the atmosphere and found the fuel cell has maximum power density at RH 20%, as a result of increasing the humidity of the membrane without causing a large concentration loss, but the impact of GDL compression was neglected. Atyabi et al. [4] discussed the effect of compression on the porosity and thickness of the GDL. They pointed out that higher compression ratio increases the electric conductivity of GDL but narrows down the diffusion path for mass transfer from channels to the catalyst layer (CL). However, the anisotropic electric and thermal conductivities of GDL are neglected, which is not reasonable considering its significant effect, especially the electric conduction [5].

In short, the literatures regarding the comprehensive influence of GDL compression rates and the open area ratios on cell performance are still rare.

Therefore, in this study, the influence of the GDL compression rate under different open area ratios is investigated using a newly developed 3D multiphase model, which includes the anisotropic electric and thermal conductivities in the in-plane and through-plane directions and contact resistance between GDL and BP.

## 2. NUMERICAL MODEL

### 2.1 Computational domain

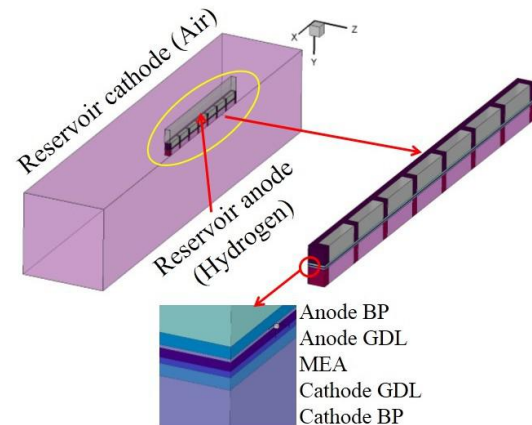


Fig.1 Computational domain

In the conventional window-based AB-PEMFC, the current collectors at cathode and anode are different. After the fuel cell assembling, the pre-tightening force will inevitably lead to the difference in GDL compressions. By using the same grid plate, the view that assume the GDL compression rates at anode and cathode are consistent is reasonable. The structure is generally used just as cathode plate in past studies.

A repeating unit is selected for calculation and symmetrical boundary conditions are used to improve calculation efficiency. When modeling the cathode, an air domain called reservoir cathode is created [6], thus

the environment that is not disturbed by other external factors around the cathode inlet is simulated, for instance, the temperature and the pressure. There is a domain that is named reservoir anode built at anode, the anode inlet is on the side wall of the reservoir, then the incoming hydrogen is distributed to each grid for the immediately reaction.

## 2.2 Governing equations

The 3D multiphase CFD model includes a group of governing equations, which are based on the first conservation law. The governing equations are given below:

$$\frac{\partial}{\partial t}(\varepsilon(1-s)\rho_g) + \nabla \cdot (\rho_g \mathbf{u}_g) = S_m \quad (1)$$

$$\begin{aligned} \frac{\partial}{\partial t} \left( \frac{\rho_g \mathbf{u}_g}{\varepsilon(1-s)} \right) + \nabla \cdot \left( \frac{\rho_g \mathbf{u}_g \mathbf{u}_g}{\varepsilon^2(1-s)^2} \right) = -\nabla P_g + \mu_g \nabla \cdot \left( \nabla \left( \frac{\mathbf{u}_g}{\varepsilon(1-s)} \right) + \nabla \left( \frac{\mathbf{u}_g^T}{\varepsilon(1-s)} \right) \right) \\ - \frac{2}{3} \mu_g \nabla \left( \nabla \cdot \left( \frac{\mathbf{u}_g}{\varepsilon(1-s)} \right) \right) + S_u \end{aligned} \quad (2)$$

$$\frac{\partial}{\partial t}(\varepsilon s_g \rho_g Y_i) + \nabla \cdot (\rho_g \mathbf{u}_g Y_i) = \nabla \cdot (\rho_g D_i^{\text{eff}} \nabla Y_i) + S_i \quad (3)$$

$$\frac{\partial}{\partial t}(\rho_l \varepsilon s) = \nabla \cdot \left( \rho_l \frac{K k_1}{\mu_l} \nabla P_l \right) + S_l \quad (4)$$

$$0 = \nabla \cdot (\kappa_e^{\text{eff}} \nabla \varphi_e) + S_e \quad (5)$$

$$0 = \nabla \cdot (\kappa_{\text{ion}}^{\text{eff}} \nabla \varphi_{\text{ion}}) + S_{\text{ion}} \quad (6)$$

$$\begin{aligned} \frac{\partial}{\partial t}(\varepsilon s_l \rho_l C_{p,l} T + \varepsilon s_g \rho_g C_{p,g} T) + \nabla \cdot (\varepsilon s_l \rho_l C_{p,l} \mathbf{u}_l T + \varepsilon s_g \rho_g C_{p,g} \mathbf{u}_g T) \\ = \nabla \cdot (k^{\text{eff}} \nabla T) + S_T \end{aligned} \quad (7)$$

Specifically, the mass and momentum equations describe the gas flows. The transport of gaseous reactants is described by the species equation. The liquid pressure equation describes the capillary pressure that drives the liquid phase flowing in the porous electrode, such as MPL. The transport of electrons and protons is described by the electric potential and ion potential equations, respectively. Heat generation of the fuel cell is added as a source term in the energy equation. For the more details refer to the previous literature [7].

## 2.3 Inclusion of GDL compression

In this study, the GDL is assumed to be uniformly deformed. As the GDL compressibility changes, the physical parameters of GDL also change, including

electrical conductivity, thermal conductivity, permeability, and porosity and so on. It is worth noting that the anisotropic transport properties, such as electric and thermal conductivities, are also taken into account in GDL, which is rarely studied in 3D simulation. The mathematical expressions of GDL properties is shown as follows [8]:

$$\frac{\delta_{\text{original}} - \delta_{\text{new}}}{\delta_{\text{original}}} = 0.449 \left[ 1 - \exp \left( -1.063 \frac{P_c}{P_c^*} \right) \right], P_c \leq 1 \text{MPa} \quad (8)$$

$$\varepsilon_{\text{new}} = 1 - (1 - \varepsilon_{\text{original}}) \frac{\delta_{\text{original}}}{\delta_{\text{new}}} \quad (9)$$

$$\frac{k_{\text{eff}}}{k_s} = \begin{cases} 1 - 0.975(1-\varepsilon)^{-0.002} \exp[0.865(1-\varepsilon)] \left[ \frac{3\varepsilon}{3-(1-\varepsilon)} \right] & \text{through-plane} \\ 1 - 0.997(1-\varepsilon)^{-0.009} \exp[0.344(1-\varepsilon)] \left[ \frac{3\varepsilon}{3-(1-\varepsilon)} \right] & \text{in-plane} \end{cases} \quad (10)$$

$$\frac{\kappa}{d^2} = 0.012 \varepsilon \left[ \frac{\pi^2}{16(1-\varepsilon)^2} - \frac{\pi}{2(1-\varepsilon)} + 1 \right] \left[ 1 + 0.72 \frac{1-\varepsilon}{(\varepsilon-0.11)^{0.54}} \right], d = 9.3 \mu\text{m} \quad (11)$$

$$\frac{\sigma_{\text{eff}}}{\sigma_s} = (1-\varepsilon)^m, \quad m = 3.4 \quad (12)$$

$$D_{\text{eff}} = \varepsilon^{1.5} (1-s)^{2.5} D_0 \left( \frac{P_0}{P} \left( \frac{T}{T_0} \right)^{1.5} \right) \quad (13)$$

It should be noted that the correlation between clamping pressure and GDL strain follows the formula (8) when clamping pressure is smaller than 1MPa, which meets the compression range of GDL in practical applications of 15%~30%. And other parameters are related to the porosity of GDL as shown in (9-13).

## 2.4 Boundary conditions

The pressures are set to be constant and equal to the operating pressure both at anode and cathode in this study. The mass flow rate is specified at anode,

$$m_a = \frac{\rho_g^a I \xi_a A_{\text{act}}}{2 F C_{\text{H}_2}} \quad (14)$$

$$C_{\text{H}_2} = \frac{P_{\text{g,out}}^a + \Delta P_g^a - R H_a P_{\text{sat}}^a}{RT} \quad (15)$$

Unlike the traditional active air supply, the cathode of AB-PEMFC is directly open to air. Through natural convection, oxygen is transferred from the cathode current collector to the GDL. Hence the calculation domain needs to extend beyond the geometrical configuration to the air domain to ensure that the pressure at the cathode inlet is equal to the

undisturbed ambient pressure. As a result, the boundary condition is free pressure condition at cathode side after adding enough reservoir.

### 3. RESULTS AND DISCUSSION

#### 3.1 Model validation

Two sets of experimental data are selected for validation. The difference between the two sets of data is very little, because the AB-PEMFC is operating at ambient temperature and the amount of hydrogen consumed is relatively small, as a result, changing the anode RH has little effect on performance. However, the numerically calculated voltage is higher than the experimentally measured voltage, especially when the current density is higher than  $480 \text{ mA cm}^{-2}$ . While at low current density, the experimental value is larger.

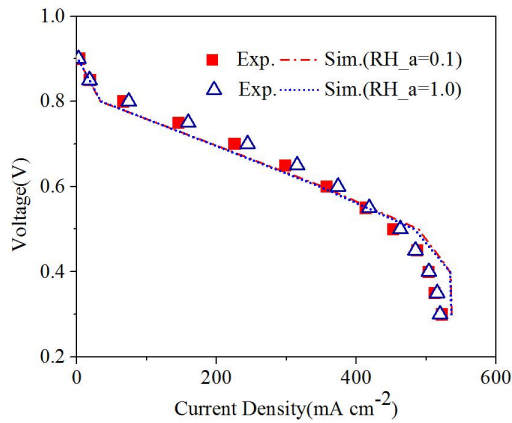


Fig. 2 Comparison of simulation results with experiment data

Fig. 2 compares two polarization curves at different anode relative humidities (298.15 K, 10% RH, 100% RH) between simulation and experiment. The error bars in Fig.2 represent  $\pm 8.7\%$  error, it means that the numerical model was validated in all cases.

#### 3.2 Effect of compression rates and open area ratios

On the basis of this model, Fig.3 shows the polarization curves of the same AB-PEMFC (open area ratio of 55%) under 15%, 17%, 30% three GDL compression rates and that neglected considering GDL compression. As the GDL compression rate increases, the physical properties of GDLs, such as the porosity, would be greatly influenced that in turn affects the overall performance of cell. The cell obtains the maximum power density when the compression rate is 17%. In addition, ignoring GDL compression significantly underestimates the cell performance.

The effects of the cathode open area ratio on performance of the AB-PEMFCs were examined. Fig. 4

shows the current density at compression rates of 15% and 30% with different cathode open areas from 28% to 80% (308.15K, 20%RH).

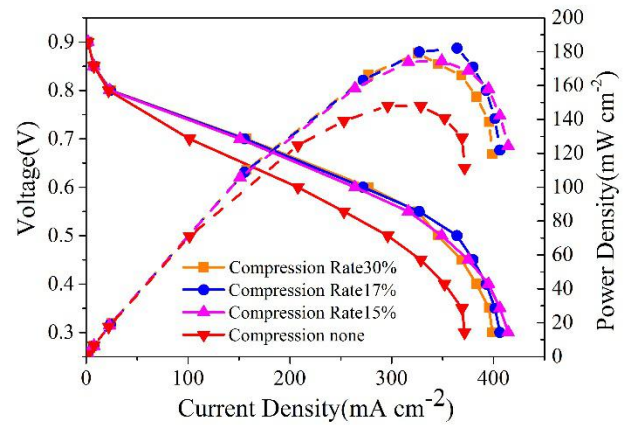


Fig. 3 Effects of GDL compression rate on cell performance

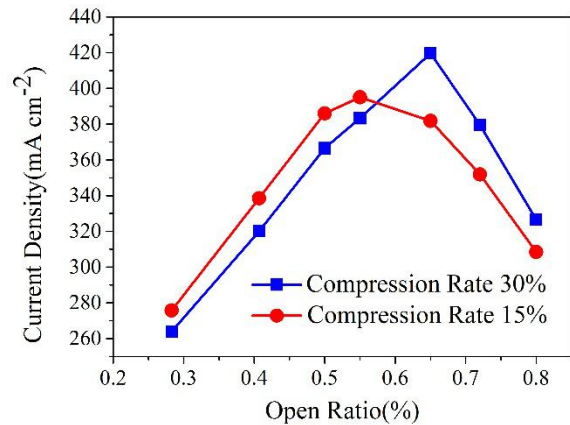
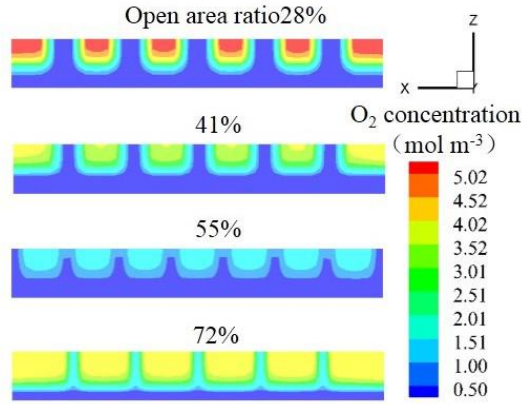


Fig. 4 Effects of the open area ratio on cell performance at GDL compression rates of 15% and 30%

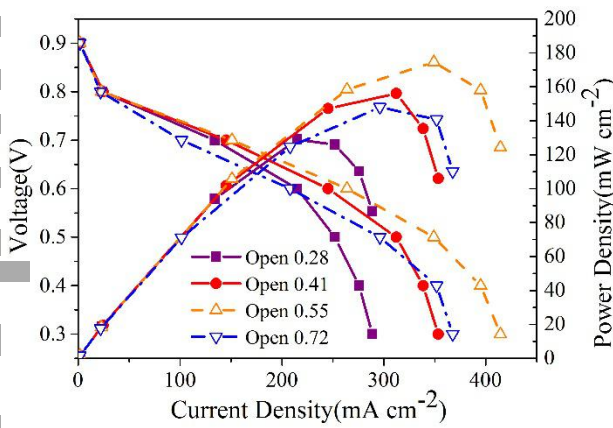
It is notable that the current density does not increase monotonically with the increase of the cathode open area. When it increases from 28%, the current density also increases, reaching a peak value of  $460.26 \text{ mA cm}^{-2}$  at the open area ratio of 55%. Subsequently, the open area ratio continues to increase, and performance of AB-PEMFC began to decline. At compression rate of 30%, similar results were obtained. Moreover, when the GDL compression rate is 15%, the optimal open area ratio is 55%, and the maximum open area ratio is 65% as the compression rate increases to 30%.

Fig.5 shows the distribution of the oxygen concentration of the cathode CL and the polarization curves with the open area ratio from 28% to 72%. Fig. 5(a) shows that the oxygen concentration is higher at the open area, which enhances the electrochemical

reaction rate, while it is lower at the contact position of the electrode plate and the GDL.



(a)



(b)

Fig.5 Effects of the open area ratio on the (a) oxygen concentration in the cathode CL (b) cell performance

Since the GDL in the open area contact with the air directly, it is beneficial to the transport of oxygen. That needs to be transported through the pores inside the GDL at the non-open area, as a result, the concentration is relatively low, which will slow down the electrochemical reaction rate.

At the same time, the increasing of the open area ratio results in a more uniform distribution of oxygen concentration. When the open area is from 28% to 72% as shown in Fig. 5(b), the polarization curves show a difference between four kinds of open area ratios. As mentioned earlier, the performance of AB-PEMFC is not directly proportional to the open area ratio, the maximum power value is obtained when the open area ratio is about 55%.

#### 4. CONCLUSIONS

In this study, the influence of GDL compression rate on the performance of AB-PEMFC under different open area ratios are studied in detail through a 3D multiphase CFD model. The main conclusions are as follows:

- (1) The cell performance is not directly proportional to the open area ratio and the best performance is obtained at a certain value. In this study, the best open area ratio for the AB-PEMFC in this study is about 55%.
- (2) For the case study in this paper, the fuel cell has the maximum power density when the compression rate of GDL is around 17%. As the compression rate increases, the cell performance increases first and then decreases.
- (3) The GDL compression rate has significant influence on the optimal open area ratio for maximum cell performance, and the larger the compression rate is, the larger the value of optimal open area ratio.

#### ACKNOWLEDGEMENT

This research is supported by the China-UK International Cooperation and Exchange Project (Newton Advanced Fellowship) jointly supported by the National Natural Science Foundation of China (Grant No. 51861130359) and the Natural Science Foundation for Outstanding Young Scholars of Tianjin (grant No. 18JJCJC46700).

#### REFERENCE

- [1] Zhang G, Jiao K. Journal of Power Sources, 2018: 120-133.
- [2] Ying W, Sohn Y, Lee W, et al. Journal of Power Sources, 2005, 145(2): 563-571.
- [3] Jeong S U, Cho E A, Kim H J, et al. Journal of Power Sources, 2006, 158(1): 348-353.
- [4] Atyabi S A , Afshari E , Wongwises S , et al. Energy, 2019, 179:490-501.
- [5] Zhang G , Fan L , Sun J , et al. International Journal of Heat & Mass Transfer, 2017, 115:714-724.
- [6] Ying W , Yang T H , Lee W Y . Journal of Power Sources, 2005, 145(2):572-581.
- [7] Zhang G, Wu J, Wang Y, et al. International Journal of Heat and Mass Transfer, 2020.
- [8] Yan X , Lin C , Zheng Z , et al. Applied Energy, 2020, 258.